Structure
Article

The Crystal Structure of the MAP Kinase LmaMPK10 from *Leishmania Major* Reveals Parasite-Specific Features and Regulatory Mechanisms

Sofía Horjales,[1] Dirk Schmidt-Arras,[3,6] Ramiro Rodriguez Limardo,[5] Olivier Leclercq,[3] Gonzalo Obal,[2] Eric Prina,[3] Adrian G. Turjanski,[5] Gerald F. Späth,[3] and Alejandro Buschiazzo[1,4,*]
[1]Unit of Protein Crystallography
[2]Unit of Protein Biophysics
Institut Pasteur de Montevideo, Montevideo 11400, Uruguay
[3]Unit of Molecular Parasitology and Signaling and CNRS URA 2581
[4]Department of Structural Biology and Chemistry
Institut Pasteur, Paris 75015, France
[5]Departamento de Quimica Biológica/INQUIMAE-CONICET, Facultad de Ciencias Exactas y Naturales, Universidad de Buenos Aires, Buenos Aires C1428EGA, Argentina
[6]Present address: Christian-Albrechts-University Kiel, Institute of Biochemistry, Rudolf-Höber-Str.1, 24118 Kiel, Germany
*Correspondence: alebus@pasteur.edu.uy
http://dx.doi.org/10.1016/j.str.2012.07.005

SUMMARY

Mitogen-activated protein kinases (MAPKs) are involved in environmental signal sensing. They are thus expected to play key roles in the biology of Trypanosomatid parasites, which display complex life cycles and use extracellular cues to modulate cell differentiation. Despite their relevance, structural data of Trypanosomatid MAPKs is lacking. We have now determined the crystal structure of *Leishmania major* LmaMPK10, a stage-specifically activated MAPK, both alone and in complex with SB203580. LmaMPK10 was observed to be more similar to p38 than to other human MAPKs. However, significant differences could be identified in the catalytic pocket, as well as in potentially regulatory sites in the N-terminal lobe. The modified pocket architecture in LmaMPK10 precludes DFG-in/DFG-out regulatory flipping as observed in mammalian MAPKs. LmaMPK10-nucleotide association was also studied, revealing a potential C-terminal autoinhibitory mechanism. Overall, these data should speed the discovery of molecules interfering with LmaMPK10 functions, with relevance for antileishmanial drug development strategies.

INTRODUCTION

Mitogen-activated protein kinases (MAPKs) are serine/threonine protein kinases mediating highly diverse intracellular signaling events. MAPKs, classified within the group of CMGC kinases, are usually not the direct sensor elements of extracellular stimuli (Plotnikov et al., 2011b), instead typically acting in the final steps of signaling cascades, which include several protein kinases working in sequence. MAPKs function as molecular switches showing at least two conformations, corresponding to catalytically active and inactive states. One of the requirements for activation usually involves posttranslational phosphorylation of key residues at the activation loop (Huse and Kuriyan, 2002; Kornev et al., 2006) by specific upstream MAPK-kinases (MKKs).

Pathogenic *Leishmania spp.* are protozoan Trypanosomatid parasites that cause human leishmaniasis. They alternate between the motile, insect-borne promastigote form and the vertebrate nonmotile amastigote stage, which proliferates inside host macrophages causing the disease (Neuber, 2008). Stage-specific signaling proteins sense extracellular cues and regulate downstream cascades, eventually related to virulence and pathogenicity. As a direct consequence of these stage-specific modifications, dramatic changes in phosphoprotein abundance and phosphorylation patterns are observed during promastigote to amastigote differentiation, to a great extent mediated by protein kinases and phosphatases that act in a stage-specific way (Morales et al., 2007, 2008).

Although MAPK signaling in the host cells has been long identified as an important process during *Leishmania* infection (Bhattacharya et al., 2011; Yang et al., 2010), much less attention has been given to the parasite's own MAPKs. According to genomic analyses, there are 17 putative MAPKs in *Leishmania spp.*, being thus one of the more expanded protein kinase families when compared to mammalian proteomes (Naula et al., 2005; Parsons et al., 2005). *Leishmania* MAPKs are involved in environmental sensing (Brumlik et al., 2011; Morales et al., 2007, 2008; Wiese, 1998) and flagella biogenesis (Bengs et al., 2005; Rotureau et al., 2009; Wiese, 2007), regulating the parasites' adaptive response pathways. Little is known on the molecular mechanisms involved in regulating protein kinase activation in Trypanosomatids. In terms of structural data, only one three-dimensional (3D) structure of a trypanosomatid protein kinase has been reported (Ojo et al., 2011), which is not a MAPK. This scenario is in striking contrast with the tremendous progress in the field of human kinases, including biologically relevant members of the ERK, p38, and JNK families, among the most-studied MAPKs. Extensive structural work on these protein

targets have unveiled specific active/inactive switching, as well as molecular details of protein:substrate and protein:protein association patterns (Huse and Kuriyan, 2002). These biologic insights have also guided several successful drug development efforts (Johnson, 2009; Simard et al., 2009). Considerable experimental work is thus needed concerning MAPK signaling in Trypanosomatids, as a number of distinctive biological features of these protozoa argue against simple extrapolations from data on higher eukaryotes. Trypanosomatids do not carry on classical transcriptional regulation (Kramer, 2012), hence typical transcription factors are not expected to be MAPK substrates; no genes coding for tyrosine kinases or SH2-domain containing adaptor proteins have been identified in the genomes, raising the question on upstream sensing; and yet, too few MAPKKs can be identified contrasting with the large number of putative MAPKs (Parsons et al., 2005), suggesting alternative MAPK activation mechanisms. Structural biology approaches focused on MAPKs from pathogenic Trypanosomatids seems thus pertinent to unveil specific regulatory mechanisms, valuable as well within serious drug discovery efforts.

We have previously shown through comparative phosphoproteomics that a limited subset of the MAPKs in *Leishmania major* (LmaMPKs) become phosphorylated when differentiating from promastigotes to the amastigote stage (Morales et al., 2007, 2008). LmaMPK4, LmaMPK7, and LmaMPK10 have thus been pinpointed as candidate regulators of parasite differentiation and survival inside host cells. Protein kinase activity studies revealed that the amastigote-specific phosphorylation of LmaMPK10 correlates to its own activation within the amastigote stage (Morales et al., 2007, 2008), activity that proved to be sensitive to SB203580 inhibition, a compound known to inhibit p38 in a specific way. LmaMPK10 has also been shown to be a protective antigen against *Leishmania* infection in an experimental animal model (Kumari et al., 2011).

Here, we present the crystal structures of apo LmaMPK10 (1.95Å resolution), as well as bound to the p38-specific inhibitor SB203580 (2.65Å), using a construct that lacks the last 46 amino acids at the C terminus. To the best of our knowledge, this is the first report unveiling the molecular structure of a Trypanosomatid MAPK with near-atomic resolution. At the structural level, LmaMPK10 is more similar to the human MAPK p38α than to other human protein kinases. However, differences in the catalytic pocket and within the N-terminal lobe are readily identified. In particular, noncanonical secondary structure elements are observed, as well as a series of distinctive amino acid residues, different from the conserved canonical sequences, occupying key positions in the structure. Among these, a particularly important motif in the regulation of protein kinases (the DFG motif) is modified in LmaMPK10 resulting in structural constraints for the otherwise well-known phenylalanine-mediated regulatory mechanism (Phe-in/out flipping). Thermodynamic studies of nucleotide binding did not allow the quantification of the ATP-binding association constant but did reveal nanomolar affinity for the binding of SB253080, a human p38-specific inhibitor. Fluorescence-based thermal shift assays further confirmed this trend. The analysis of the association constants, comparing full-length LmaMPK10 and a truncated variant that lacks a parasite-specific C-terminal extension, suggests that a structural mechanism of nucleotide-binding autoinhibitory interference exists, conveyed by that terminal self-peptide.

RESULTS AND DISCUSSION

LmaMPK10 Expression and Characterization

Recombinant full-length LmaMPK10 from *Leishmania major* was expressed in *Escherichia coli*, but poorly diffracting crystals were obtained after extensive crystallogenesis condition screenings. Limited proteolysis and mass spectrometry analysis of LmaMPK10 confirmed the presence of a ~40-residue C-terminal extension that is sensitive to proteolytic digestion, suggesting it might include an unstructured or more flexible segment. Accordingly, a truncated form lacking the last 46 residues (LmaMPK10ΔC) was engineered, produced in recombinant form, and purified to homogeneity, allowing us to obtain crystals with significantly better X-ray diffraction quality.

Enzyme-coupled activity assays (Schindler et al., 2000) were performed to quantify ATP-dependent phosphorylation kinetics of LmaMPK10 and LmaMPK10ΔC (methods details in the Supplemental Experimental Procedures, available online). Neither one of these two constructs catalyzed detectable activities under these conditions, within the method's sensitivity limits (Technikova-Dobrova et al., 1991), using a well-characterized protein kinase (*Mycobacterium tuberculosis* PknB) as positive control. The PknB-catalyzed phophotransfer in these conditions revealed a k_{cat} of 0.1 s^{-1}, considering ~250 nM product as a rough minimum detection limit (Technikova-Dobrova et al., 1991), LmaMPK10 displays a $k_{cat} < 2.10^{-6}$ s^{-1}. Substitution of Mg^{2+} by Mn^{2+}, or even avoiding cations altogether, did not result in detectable catalytic levels. Using the same experimental approach, the ATPase and the kinase activities of p38α have shown to be coupled (Chen et al., 2000), and unphosphorylated p38α (or even monophosphorylated on Tyr within the activation loop) shows undetectable activity (Zhang et al., 2008). Phosphorylated variants of recombinant LmaMPK10 and LmaMPK10ΔC were identified by liquid chromatography-coupled electron spray mass spectrometry (Supplemental Experimental Procedures), after incubation with ATP (including both monophosphorylated variants on the THY motif of the activation loop), but this did not result in detectable increase of protein kinase activity (data not shown). A detailed characterization of these phosphopeptides was thus not further considered, coming from *E. coli* their biological relevance is questionable. Recombinant LmaMPK10 is most probably purified in a nonactive state, and the specific *Leishmania* MKK that phosphorylates LmaMPK10 upstream (leading to a double phosphorylated activation loop profile) is yet to be identified.

Overall Structure of apo LmaMPK10ΔC

LmaMPK10ΔC was crystallized, and its structure was solved with X-ray diffraction techniques. Molecular replacement using human p38α as a search probe (Protein Data Bank [PDB] ID code 3HV3) gave the best rotation function contrast, allowing to refine the model to 1.95Å resolution (Table 1). Final electron density maps display excellent quality in the C-terminal lobe (see below for detailed structure description) (Figure 1A) and weaker signal to noise levels in the N-terminal lobe and particular segments. The model was built, including most of the amino

Table 1. X-Ray Diffraction Data Collection and Refinement Statistics

	LmaMPK10ΔC	LmaMPK10ΔC + SB203580
Space group	P 4_3 2_1 2	P 4_3 2_1 2
Protein molecules per asymmetric unit	1	1
Solvent content (%)	52.4	52.6
Wavelength (Å)	1.5418	1.5418
Data Resolution (Å)[a]	28.73–1.95 (2.06–1.95)	43.1–2.63 (2.77–2.63)
Measured reflections	110,807	59,508
Multiplicity[a]	3.5 (3.5)	4.5 (4.5)
Completeness (%)[a]	98.3 (97.4)	97.7 (84.3)
R_{meas} (%)[a,b]	5.0 (53.7)	9 (58.7)
$<I/\sigma\sigma(I)>$[a]	15.8 (1.4)	13.7 (1.3)
a = b (Å)	81.26	80.9
c (Å)	129.38	131.02
Refinement resolution (Å)	28.73–1.95	43.1–2.65
R_{cryst}[c] [N° refs]	0.192 [29,996]	0.215 [12,184]
R_{free}[c] [N° refs]	0.224 [1,638]	0.241 [997]
Rms bonds (Å)	0.011	0.008
Rms angles (°)	1.07	1.04
Protein nonhydrogen atoms	2,706	2,422
Water atoms	193	59
Ligand atoms	–	27
Mean B factor: overall (Å^2)	53.6	76.1
Mean B factor: main chain (Å^2)	51.9	75.2
Mean B factor: side chains (Å^2)	55.5	78.1
Mean B factor: waters (Å^2)	52.7	52.7
Mean B factor: ligand (Å^2)	–	86
Map versus model correlation coefficient (Overall/local)[d]	0.84/0.88	0.82/0.87
N° residues in Ramachandran plot regions[e] (Allowed/favored/outliers)	337/325/0	297/282/0
Protein Data Bank ID code	3PG1	3UIB

[a]Values in parentheses apply to the high-resolution shell.
[b]$R_{meas} = \sum_h \sqrt{N_h/(N_h-1)} \sum_i |I_i - \langle I \pm \rangle| / \sum_h \sum_i I \pm$; N_h, multiplicity for each reflection; I_i, the intensity of the i^{th} observation of reflection h; $< I >$, the mean of the intensity of all observations of reflection h, with $I \pm = 1/N_h \sum_i (I_{(-)}$ *or* $I_{(+)})$; $\sum_h$ is taken over all reflections; $\sum_i$ is taken over all observations of each reflection.
[c]$R = \sum_h |F(h)obs - F(h)calc| / \sum_h |F(h)obs|$; R_{cryst} and R_{free} were calculated using the working and test hkl reflection sets, respectively.
[d]Calculated with Phenix get_cc_mtz_pdb (Adams et al., 2010).
[e]Calculated with Molprobity (Chen et al., 2010).

acids, according to reliable electron density features, thus excluding the first 4 N-terminal residues, the last C-terminal one, and the zone spanning residues 180 to 194. The latter segment corresponds to the activation loop, and although electron density was visible, it was not sufficiently clear to allow for confident interpretation, instead suggesting high flexibility and/or the presence of alternative conformations that are not distinguishable at this resolution. The side chains of fourteen residues have also been excluded because of similar reasons.

The structure of LmaMPK10ΔC displays the canonical eukaryotic-like protein kinase (ePK) fold, which includes a smaller N-terminal lobe, including a central β sheet and a larger, mostly helical C-terminal domain, both connected by two hinge segments (Figure 1B; Figure S1A). The N-lobe includes the structurally conserved 5-stranded antiparallel β sheet in the core (β1–β5), surrounded by three solvent-exposed α helices: the strictly conserved αC, the C-terminal α11, right after the second hinge segment, and, at the very beginning of the protein, α1, a secondary structure element unique to this MAPK (Figure 1B). Also atypical is a small insertion of seven residues in the N-terminal lobe that folds into a β-hairpin (amino acids 55–63; noncanonical βIV–βV; see PK10 insertion in Figure 1B and Figure S1). Well-exposed to the solvent, this β-hairpin immediately precedes helix αC. The C-terminal lobe is better conserved as judged by its canonical, mainly helical secondary structural elements, except for a small 3-stranded β sheet (β6–β8), well-conserved and located close to the substrate binding site.

The first interlobal hinge (hinge I; residues 113–116) is short, just after the so-called "gatekeeper" residue (Thr 112), important in allowing for nucleotide binding into the ATP-pocket. Hinge II is instead a long loop (residues 329–345), connecting the C-terminal lobe to the last α helix (α11), which is folded back onto the N-terminal lobe, a typical feature of MAPKs. Eleven helices are thus observed in all, not taking into account short helical segments (280–284, 303–307, and 324–329) or yet the nonregular, twisted helical section 195–205, just after the activation loop. The conserved helices αC through αI, were labeled according to a widely used secondary structure nomenclature (Scheeff and Bourne, 2005). Between αG and αH, two α helices are inserted forming the MAPK insertion MKI (α helices α7 and α8), typical of the CMGC group of protein kinases (Kannan and Neuwald, 2004). A Ser-Pro-Ser motif (SPS) within the MKI has been shown to be important as a noncanonical nuclear localization signal in ERK1/2 (Chuderland et al., 2008; Plotnikov et al., 2011a), whose subcellular localization appears to be regulated by Ser phosphorylation. The LmaMPK10 MKI also harbors an SPS motif, although it is not structurally equivalent to the one in ERK (which is substituted in LmaMPK10 by Thr-Pro-Lys). This modified motif in LmaMPK10 is seen located on the opposite side of the MKI, equally well-exposed to the solvent.

A strictly conserved glutamate on αC (Glu78 according to LmaMPK10 numbering), is well known to establish a salt bridge with a lysine in β3 (Lys51), when protein kinases are locked in their active conformation (Taylor and Radzio-Andzelm, 1994). In this structure of apo LmaMPK10ΔC, the carboxylate group of Glu78 is located 3.9 Å away from the amino group on the Lys51 side chain, which is observed also to be mobile, according to weak electron density and high B factors, indicating that this interaction is not strong (Figure 1C). Arg157 (included within the conserved HRD motif), the following catalytic Asp158, and

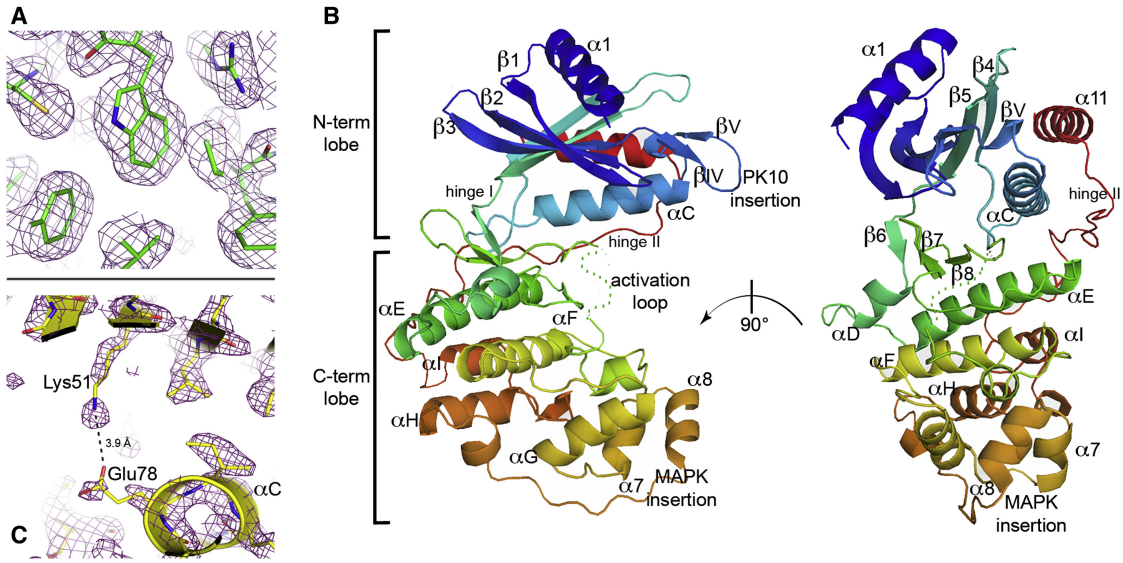

Figure 1. Overall 3D Structure of LmaMPK10ΔC in Its apo Form

(A) Fully refined electron density map (sigmaA-weighted 2mFobs-DFcalc, contoured at 1.5σ) with superposed amino acids in stick representation as a reference of the final model.

(B) Cartoon representation of the full model, viewed from two orientations (the right panel is rotated 90° according to a vertical axis in the plane of the paper, with respect to the left panel); the model is colored according to a blue-to-red ramp, indicating the N-terminal to C-terminal direction of the polypeptide; secondary structure elements and particular LmaMPK10-specific motifs are labeled.

(C) Zoom-in showing the refined electron density (sigmaA-weighted 2mFobs-DFcalc, contoured at 1σ) corresponding to residues Lys51 and Glu78. The salt bridge distance is marked in angstroms. Note the weak electron density of these interacting amino acids.

See also Figure S1.

Asn163, are located in the catalytic loop, and are all well resolved in the electron density maps.

Comparing LmaMPK10 to human orthologs, the closest relatives are ERK1/2 and p38α (40% and 36% identity, respectively). Despite the marginally higher sequence similarity with ERK1/2, on structural grounds the relatedness is slightly more important with p38α (DALI Z scores of 35.6 with p38α [PDB ID code 3GFE] versus 34.1 with ERK2 [3ERK]), well above other homologous kinases displaying DALI Z scores <30, such as JNK3 (2P33), CDK2 (1JST), and GSK3 (1H8F). These structural differences can be identified in overall superpositions with p38 versus ERK (Figure S1B), also explaining why p38α models resulted in better solutions on the initial molecular replacements searches. The most important changes can be observed in the N-terminal lobe, wherein the position of αC and a few loops are more similar between LmaMPK10 and p38α than to others. At difference with the human counterparts, the electrostatic potential mapped onto the solvent accessible surface of LmaMPK10, highlights a large electronegative patch on the opposite side of the ligand binding cleft (Figure S1C).

The heterogeneous electrostatic charge distribution on the surface, as well as the presence of unique secondary structure elements well-exposed to the solvent, are compatible with scaffolding of protein:protein associations, currently under investigation using structure-guided mutant constructs expressed in *Leishmania*. Helix α1 replaces the more typical two-stranded β sheet found in most MAPKs. This could be a feature common to several trypanosomatid PKs, because it is also observed in the other available 3D model of a protein kinase from *Leishmania*, glycogen synthase kinase GSK (Ojo et al., 2011), although in GSK it is found in a ~90° rotated orientation. The topological position of the β-hairpin just preceding αC, invites to the hypothesis of a potential regulatory role, because interactions with partner molecules at this site could directly affect the position of αC (Figure 1B), a key helix in kinase activation regulation.

LmaMPK10-Specific Sequence Features

The LmaMPK10 sequence and 3D structure were used as queries in multiple sequence alignments in order to locate conserved and variable features (Figure S2). As expected, the ePK domain is readily detectable, including the 12 highly conserved ePK motifs (Manning et al., 2002) (Figure 2A). Most of the residues that define the protein kinase CMGC group (Kannan and Neuwald, 2004) are indeed conserved in LmaMPK10. Among these, three positions display substitutions: Met205 (which is a Leu in typical MAPKs), Phe210 (substituting a Tyr), and Arg234 (substituting a Pro).

Although the strictly conserved residues in ePKs (Kannan et al., 2007) are present in LmaPK10, there are a few point substitutions in particularly intriguing positions. These unique atypical features are well conserved only among trypanosomatid LmaMPK10 orthologs (Figure S2) and are not present in any one of the other 16 MAPKs from *Leishmania*. These residues are located within conserved loops or segments known to play important functional roles in MAPKs (Figure 2B). Focusing on the most important, and following their sequential order in the protein, these key positions fall in the P loop between strands β1 and β2; the HRD motif in the catalytic loop; the DFG triad

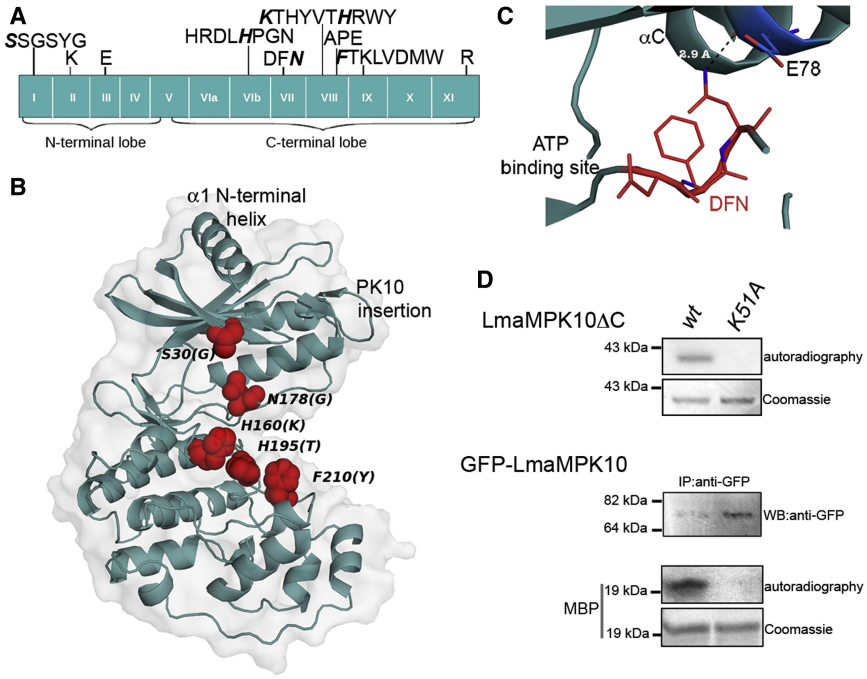

Figure 2. LmaMPK10-Specific Features in Key Functional Positions

(A) Schematic representation of the full sequence of LmaMPK10, showing the relative positions of the 12 conserved ePK motifs (indicated in roman letters). A selection of highly conserved residues are labeled. Among these, some of the residues that are not conserved in LmaMPK10 and trypanosomatid orthologs are marked in italic bold. The return of the last C-terminal portion toward the N-terminal lobe is not indicated for clarity.

(B) Cartoon representation of LmaMPK10ΔC, superposed within the transparent solvent accessible surface. For clarity, only five LmaMPK10-specific point substitutions are marked as red spheres.

(C) A close-up of the modified DFG motif, which has evolved to DFN in LmaMPK10. The H-bond that links the asparagine side chain to the key Glu78 in the αC is indicated. Note the phenylalanine in the "Phe-in" flipped position, resembling the configuration of kinases in the active state. The ATP-binding site is labeled for spatial reference.

(D) SDS-PAGE separations of LmaMPK10 and variants, revealing autokinase and phosphotranferase activities at the expense of [γ^{32}P]-ATP. The autophosphorylation capacity of pure recombinant LmaMPK10ΔC is shown on the top of the panel, comparing the *wt* versus a Lys51Ala kinase-dead mutant. On the bottom part, phosphotransfer from ATP to myelin basic protein (MBP; ~21 kDa) is detected using the full-length *wt* LmaMPK10, fused to GFP (allowing for immunoprecipitation from *L. donovani* amastigotes using anti-GFP antibodies [IP:anti-GFP]). Coomassie staining is very weak for immunoprecipitated GFP-LmaMPK10 and GFP-LmaMPK10-Lys51Ala, equivalent quantities were confirmed by western blotting as indicated (WB:anti-GFP).

See also Figure S2.

that participates in cation-binding and catalytic regulation control; and finally, the so-called activation loop, just after the DFG motif, finishing in the sequence APE.

(1) The P loop (residues 30–34), including the conserved GXGXXG sequence, is directly implied in nucleotide substrate positioning. In LmaMPK10 it contains Ser30 replacing the first conserved Gly residue.

(2) In ERK2 the phosphotransfer reaction is catalyzed by Asp147 (included in the conserved motif HRD), which acts as a base, and Lys149, which interacts with the γ-phosphate along the reaction pathway, providing the right positioning of the ATP and stabilizing the transition state (Turjanski et al., 2009). In LmaMPK10, the catalytic Asp corresponds to Asp158, but the conserved Lys is substituted by a His160. This His residue is thus occupying a key position toward the ATP substrate-binding site, very close to, and pointing in the same direction as the catalytic Asp158. A histidine in this position is present in very few members of the ePK family, particularly in members recently classified as ELKs (ePK like kinase family) from prokaryotes (Kannan et al., 2007). ELKs display functional and sequence diversity and are not well characterized. Their substrates include proteins and small molecules (lipids, sugars, and amino acids) and appear to have regulatory functions.

(3) After the HRD motif, the catalytic loop displays yet another unusual substitution in position 173, where the canonical lysine is replaced by a threonine.

(4) Perhaps the most striking substitution, given its functional importance, concerns the conserved DFG motif, which delimits the beginning of the activation loop (Figure 2C). Asn178 in LmaMPK10 substitutes the expected Gly in this triad element. This glycine is directly involved in the key regulatory switch between DFG-in (active) and DFG-out (inactive) conformations in ePKs (Kornev et al., 2006; Pargellis et al., 2002), linked to interlobe movement and active-site accommodation for catalysis. The presence of an Asn at position 178 in LmaMPK10 results in important implications for the "on-off" switching. Asn178 makes the main chain of this triad more rigid, because it is stabilized through an H-bond to the main chain of Glu78 (Figure 2C), adding further restriction to the position of the helix αC and making the required DFG-in/DFG-out movement less likely. In the DFG-out conformation, the conserved glycine displays a combination of ϕ/ψ main-chain dihedral angles that is less probable for any other amino acid, such as the asparagine present in LmaMPK10.

(5) Residue substitutions can also be identified within the activation loop. The phosphorylatable Thr190 and Tyr192 constituting the THY motif are seen embedded in a quite unusual context in LmaMPK10. Position 189, typically a hydrophobic residue in PKs, is occupied by a lysine in LmaMPK10 (not included in the model because of activation loop mobility and lack of electron density), and

(6) the highly conserved Thr at position 195 within the TRWY sequence, is substituted by a His.

(7) A more subtle substitution at position 210, involves a Tyr to Phe change, which is nevertheless worth mentioning, given the functional importance of the Tyr OH group in kinase on/off switching in many CMGC kinases (Kannan and Neuwald, 2004), principally via stabilization of the key Thr in the activation loop, once it becomes phosphorylated in the PK-active state.

Six point mutations in LmaMPK10 (S30G, H160K, N178G, K189M, H195T, and F210Y), reverting to the ePK-typical residues, were generated and the recombinant proteins purified. No gain of protein kinase activity in autophosphorylation or surrogate substrate assays was revealed (data not shown). The possibility of synergic effects, by combination of several or all mutations simultaneously, cannot be excluded and merits further structural and biochemical characterizations, currently underway.

At this stage, taking into account the fact that LmaMPK10 protein kinase activity was not detected and that several highly conserved residues are seen to be changed, we considered the possibility that LmaMPK10 would be a pseudokinase. With this aim we used [γ^{32}P]-ATP as phosphodonor substrate, increasing the sensitivity of the method. We first analyzed the autophosphorylation activity of the construct used for structural studies, comparing wild-type LmaMPK10ΔC with the corresponding Lys51Ala point mutant used as a catalytically dead control (Figure 2D). LmaMPK10ΔC is able to use ATP to autophosphorylate specifically, needing a competent ePK-canonical architecture (i.e., Lys51 required to establish the salt bridge with Glu78). We then wanted to look also at the full-length protein, in its proper biologic context, so we generated GFP-tagged versions of the *wt* and the Lys51Ala point mutant, with which *L. donovani* cells were transfected. Immunoprecipitation from soluble protein extracts of amastigote cells was performed using an anti-GFP antibody. The pulled-down material was confirmed by western blot, displaying the expected size for the GFP:LmaMPK10 fusion protein (73.9 kDa), and used as LmaMPK10 source for kinase activity assays. Autophosphorylation was undetectable, perhaps because LmaMPK10 is already phosphorylated in amastigotes, but phosphotransfer to myelin basic protein (MBP) used as a surrogate substrate was observed (Figure 2D). Once again, LmaMPK10 kinase activity was shown to be dependent on the integrity of the active site because the Lys51Ala mutation abolished phosphotransfer capacity (Figure 2D). Although LmaMPK10 catalyzed MBP phosphorylation with a much weaker activity than ERK2 (not shown), *wt* LmaMPK10 is not a pseudokinase, being able to use ATP to catalyze autophosphorylation and phosphotransfer to a surrogate peptidic substrate.

LmaMPK10 Binding of SB203580

Determining the structure of LmaMPK10ΔC in complex with a nucleotide, a nucleotide-derivative or a competitive inhibitor, constitutes an important step forward within a target-based drug discovery strategy. Soaking, as well as cocrystallization experiments, were performed using ATP, ADP, and AMP-PCP in the presence or absence of Mg^{2+} and Mn^{2+}. Despite great efforts, the resulting structures reproducibly showed no detectable occupancy of the nucleotide-binding site. We then decided to determine the binding affinities of LmaMPK10 to ATP or ATP-like molecules. Isothermal titration calorimetry was used to quantify the ATP-LmaMPK10 and ATP-LmaMPK10ΔC dissociation constants at equilibrium, but signal-to-noise ratios were too low in order to derive accurate figures. This likely reflects a weak ATP association constant, although concurrent effects linked to high heats of dilution of Mg^{2+} cannot be formally excluded. Fluorescence-based thermal shift assays (TSA) also failed to uncover ATP-LmaMPK10 association using both the full-length as well as the truncated constructs of the protein (Figures S3A and S3B). Binding was eventually detectable by using the p38-specific inhibitor SB203580 (Cuenda et al., 1995) as ligand (Figures 3A and 3B). Both the full-length kinase and its truncated version bound to SB203580 with a 1:1 stoichiometry. The associations were essentially driven by the enthalpic component. The observed dissociation constants greatly depended upon the presence of the 46-residues C-terminal extension (Table 2) as LmaMPK10ΔC showed a >30-fold increase in binding affinity. Comparative analysis of the full-length and ΔC-truncated versions of LmaMPK10 by TSA further confirmed this trend (Figure S3C).

TSA analyses revealed a further relevant feature: the full-length wild-type protein was significantly more stable than the truncated LmaMPK10ΔC (>12°C). The low quality of full-length LmaMPK10 crystals in diffracting X-rays and the identification of a proteolysis-sensitive segment within the C-terminal extension must be analyzed in the context of this greater thermal stability of the full-length protein. The most likely model would thus anticipate that an intervening loop within the C-terminal extension is mobile in solution, at least in the nonphosphorylated state of LmaMPK10. Nevertheless, part of the extension is most probably interacting with the core of the kinase, consistent both with the overall stabilizing effect, as well as with the observed autoinhibition on the ATP-binding pocket (Figure 3C). The >30-fold decrease in the SB253080 association constant when the wild-type extension is present, is saying that this extension exerts a direct interfering effect onto the nucleotidic cleft, most probably through its direct contact with the LmaMPK10 core. In support of this hypothesis, secondary structure prediction of the 46 residues C-terminal peptide gives reproducible results using different algorithms (Figure S3B). A first α helix is predicted with high confidence, including the first ~20 amino acids of the peptide, and then an intervening loop would connect to a second shorter α helix. Ab initio 3D modeling of the first 36 residues of the C-terminal peptide using PEP-FOLD (Thévenet et al., 2012) resulted in well-clustered sets of solutions, reproducibly consistent with the secondary structure predictions. Among the best resulting models, according to the program's template modeling score and energy ranking, were several that actually fit nicely through the back of LmaMPK10ΔC, directly reaching the nucleotidic cleft (Figure 3C). Although this in silico model awaits experimental proof, it illustrates plausible distances that take into account proper peptidic stereochemical constraints, while explaining the thermal stabilization and the autoinhibited behavior of full-length protein. From the C-terminal end of α11, to a midpoint within hinge I at the ATP-binding pocket, there is a ~25Å distance, closely matching the predicted length of an 18-residues, 5-turn α helix. On the other hand, this first half of the 46 amino acids C-terminal extension, presents highly charged

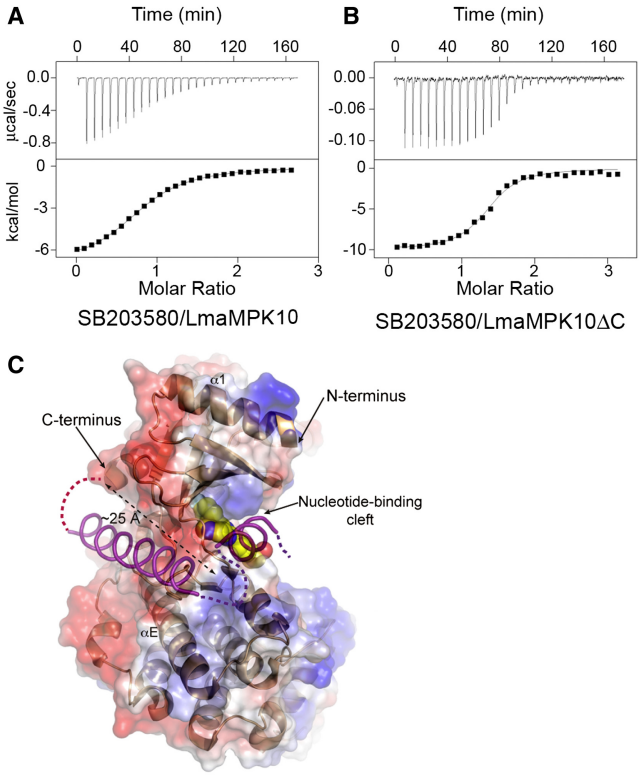

Figure 3. Thermodynamic Analysis of LmaMPK10 Binding to SB203580

(A and B) A comparison of the isothermal titration calorimetric curves between (A) full-length LmaMPK10 and (B) C-terminally truncated LmaMPK10ΔC is shown, both being titrated with the human p38-inhibitor SB203580. Top panels display raw heat fluxes (corrected for heat of dilution of both protein and inhibitor), whereas bottom panels show the integrated heat of injection (normalized to the amount of SB203580 injected). Note the similar stoichiometries in terms of inhibitor:protein molar ratios, whereas association constants change significantly (full details in the text and Table 2).

(C) Plausible model for the association of the C-terminal 46 residue extension truncated in the LmaMPKΔC construct. The 3D structure of apo LmaMPKΔC is shown as a cartoon, with the N termini and C termini indicated. Superposed, a transparent rendering of the electrostatic potential mapped onto the accessible solvent surface of the protein. The coordinates corresponding to the inhibitor SB203580 occupying the ATP-binding site, have been grafted from the LmaMPKΔC-SB203580 complex solved in this work (see Figure 4) and represented in spheres colored by atom to locate the nucleotide-binding cleft. The two predicted α-helices of the C-terminal peptide, absent in LmaMPKΔC, are shown as a violet ribbon (rendered semitransparent to highlight that it is a predicted model). Its coordinates correspond to the best scoring ab initio 3D model, which includes only the first 36 amino acids of the peptide (see the Supplemental Experimental Procedures). The connecting two residues between α11 and the C-terminal extension are depicted as red dashes; the intervening loop and the final ten residues within the peptide are marked as violet dashes. Note the distance match between the peptide's predicted first α helix with the one separating the C-terminal end of α11 and the entrance of the ATP-binding cleft.

See also Figure S3.

residues in an alternate fashion such that basic arginines can be nicely accommodated interacting with the acidic surface seen on the back of LmaMPKΔC (Figure 3C). An alternative, more sophisticated mechanism, could imply allosteric modifications triggered by the self-peptide binding away from the nucleotidic cleft, eventually also resulting in the autoinhibitory effect. It will thus be important to study if this C-terminal extension is modified in vivo (e.g., through phosphorylation, binding of molecular partners, including dimerization, or yet proteolysis events), thus linked to the physiological activation process.

Structure of LmaMPK10ΔC in Complex with SB203580 and Analysis of the Nucleotide-Binding Cleft

With this background information, we intended to solve the crystal structure of LmaMPK10ΔC in complex with SB203580, ultimately succeeding using a compound-soaking approach. The inhibitor's low solubility in water and its effect in rendering the crystals more fragile complicated this task. After screening many crystals on the basis of X-ray diffraction quality, we chose the one diffracting to highest resolution (Table 1) and solved its structure (Figure 4A) by molecular replacement using the refined apo model. Initial cycles of refinement were performed employing simulated annealing, and reciprocal space refinement was thereafter iterated with manual model rebuilding. Model building proved to be a nontrivial task, mainly because the N-terminal lobe displays vast regions not well defined in electron density. Residue fragments 1–6, 17–24, 28–33, 57–63, 97–107, and 360–361 spanning solvent-exposed loops and β strands in the N-lobe domain, as well as the activation loop residues 180–191, could not be modeled because of a lack of interpretable electron density. The side chains of 19 residues, mostly belonging to the N-lobe domain, were not included in the model for the same reasons. The B factors of those parts of the N-lobe that do fit well in the electron density maps refine to extremely high values (Figure S4), revealing important flexibility of the molecule in this lobe. This pronounced differential flexibility between both domains of LmaMPK10ΔC appears to be a particular feature, as compared to homologous MAPKs, such as p38 (Figure S4).

The nucleotide-binding site lies in the hinge region between the two lobes (Figure 4). Although the key residues involved in catalysis in ePK are conserved in LmaMPK10, several differences exist in the active site. The ligand-binding cleft displays a number of residues involved in contacts (Figure 4B), most of them establishing van der Waals interactions. Only one H-bond is observed between nitrogen atoms involving the main chain of Met115 and the inhibitor's NB1 on the pyridine ring acting as H-acceptor. Structural superposition of the apo and SB203580-bound models of LmaMPK10ΔC allowed us to focus onto inhibitor-triggered rearrangements. Tyr34 within the P loop gets closer to the ligand, indicating that the whole P loop, although not well defined in electron density, moves in, closing the ligand-binding cleft. The side chain of Asp176 is shifted, accommodating the inhibitor in place. Although Lys51 is closer to Glu78 side chain, it is still strikingly flexible, displaying low electron density for its side chain. No significant differences are detected in the C-terminal lobe. The ATP binding pocket of LmaMPK10 has a smaller cleft and a different exposed profile of the electrostatic potential on the active site's surface (Figure S4D), when compared to other MAPKs, such as human p38α and ERK2. The narrowing of the cleft as compared to p38α obeys to a tighter closure of the glycine-rich loop onto the nucleotide analog. This is linked to the unusual fact that the DFG-in configuration of apo LmaMPK10 is not changed in the

Table 2. Isothermal Titration Calorimetry Analysis of the LmaMPK10/SB203580 Interaction

Protein	Stoichiometry	Kd (μM)	ΔG (kcal.mol^{-1})	ΔH (kcal.mol^{-1})	TΔS (kcal.mol^{-1})
LmaMPK10	0.82 (0.0024)	5.3 (0.21)	−7.36 (0.021)	−7.15 (0.068)	0.21 (0.089)
LmaMPK10ΔC	1.33 (0.035)	0.16 (0.015)	−9.5 (1)	−10.3 (1.13)	−0.80 (0.088)

Values reported were obtained from the average of two independent titrations, with standard error of the mean indicated in parentheses.

SB203580-bound complex. SB203580 is known to bind and stabilize the DFG-out conformation in p38, wherein Phe169 within the DFG motif contributes to direct binding of the inhibitor. Overall, LmaMPK10 naturally binds SB203580 with an ''ERK-like'' configuration, closely resembling the profile seen in 1PME.

LmaMPK10: On/Off Switching and Activation State

The active state of ePKs requires two continuous columns or spines of stacked hydrophobic residues, the regulatory (R) and the catalytic (C) spines (Kornev et al., 2006; Taylor and Kornev, 2011). Although many different configurations are found for the inactive states of ePKs, a common theme involves breaking the R spine in one way or another. Attempts to classify the structures of LmaMPK10 as active or inactive are not clear-cut. Among the off-state traits, the protein displays an open conformation, which is seen only slightly closed when bound to the SB203580 inhibitor (Figure 4B). More importantly, no phosphorylated residues were detected. Although most of the activation loop could not be modeled, mass spectrometry analyses of the samples used for crystallization do suggest they are nonphosphorylated. The high flexibility of the activation loop on its own is not a clear signature of activation state: unphosphorylated inactive human p38α displays a well-ordered loop (PDB ID code 1P38), whereas active ERK, double-phosphorylated on the activation-loop TEY motif, also displays an ordered activation-loop conformation (2ERK). Although the distance between the side chains of Lys51 and Glu78 is consistent with a salt bridge, typical of activated ePKs, Lys51 is very mobile in our LmaMPK10 structures, strongly suggesting that this ionic interaction is not strong.

On the other hand, a continuous, unbroken, regulatory spine suggests that LmaMPK10 has been crystallized in an ''active-competent'' configuration. The presence of an asparagine (Asn178) substituting the glycine in the otherwise highly conserved DFG motif, actually stabilizes Phe177 in a ''DFG-in'' position, completing the R-spine (Leu93, Leu82, Phe177, and His156) (Figure 5A). This ''active-state'' architecture on the apo form of LmaMPK10ΔC is further stabilized through an H-bond between the side-chain of Asn178 and the main chain O of Glu78 (Figure 2C), a key residue in properly orienting αC to complete the R-spine. Flipping Phe177 to an inactive ''DFG-out'' state seems either not possible, or at least involving a high-energetic penalty, given that Asn178 does not have the necessary intrinsic flexibility on its main chain dihedral angles, a functional role uniquely ensured by a glycine (Kornev et al., 2006). Further supporting this modified behavior when compared to human MAPKs, the p38-specific inhibitor SB203580, which stabilizes the DFG-out configuration in p38α, does bind to LmaMPK10, but is not able to trigger/stabilize a DFG-out flipping in the LmaMPK10-SB203580 structure. The residues involved in building a continuous C-spine are also well positioned, constituting an active-competent architecture (Ala49, Val37, Leu165, Leu166, Ile164, Leu119, Val222, and Met226) completed by the ATP-pocket ligand SB203580 in the complexed structure (Figure 5A).

The nucleotide-bound state of LmaMPK10ΔC is only mimicked by using SB203580, as nucleotide incorporation has been elusive. Taking into account the overall extremely high B-factors, as well as the differential higher plasticity of the N-terminal lobe (Figure S4), we sought to analyze LmaMPK10's plastic propensity by molecular dynamics simulations. The apo structure was compared to the SB203580-bound, as well as to a simulated structure, where ATP was docked within the nucleotidic cleft (by superposition with the ATP-bound p38γ structure 1CM8). A similar calculation was performed with the structure of p38α (1R3C) to be used as reference. As anticipated from the crystal structures, LmaMPK10ΔC shows indeed higher flexibility than p38α, especially on the N-terminal lobe (Figure S5A). The PK10 insertion, absent in p38, is highly flexible, both in the apo and SB203580-bound models. This more plastic behavior is not rigidified when SB203580 is bound in the nucleotide-binding pocket (Figure S5B), whereas a clear stabilization is instead observed if the true ATP moiety is in place (Figure S5C). This significantly different effect of ATP with respect to SB253080 can be further scrutinized by analyzing some important details. Only with ATP bound, the P loop is anticipated to close in much more snugly onto the nucleotide moiety, correlating with a strong interaction between Lys51 and Glu78 (Figures 5B–5E; Figures S5D–S5F). The NZ atom on Lys51 is actually predicted to interact with the acidic Glu78 side chain, as well as with the α- and β-phosphates of ATP itself (Figure S5E), as has been seen in other nucleotide-bound MAPK structures (Bellon et al., 1999; Xie et al., 1998). The distance between Lys51 and Glu78 oscillates along the simulation between 3.5–8.0 Å in both the unbound and SB203580 forms (Figure S5F), measuring the distances between the NZ atom of Lys51 and the CD of the carboxyl moiety of Glu78, because the carboxyl oxygens frequently switch their interactions during the dynamics. These predicted distances in solution may thus be readily grouped in two major populations (Figure S5F), one of which corresponds to the interatomic distance observed in the X-ray structures.

Hence, although the pyrimidine ring of SB203580 occupies the position of the adenine base in ATP, completing the catalytic spine, this does not appear to be sufficient by itself to trigger the full set of modifications toward an active configuration, notably, SB203580 being deficient in stabilizing the Lys51-Glu78 ion pair (and correlated movements on the P loop and αC helix, as seen in our structure). The overall high B factors in the LmaMPK10ΔC structures and particularly high plasticity of the N-terminal lobe may be related to the fact that the C-terminal 46-residues extension is not present. Probably the first ~20 residues of this extension are part of the N-lobe core. In any case,

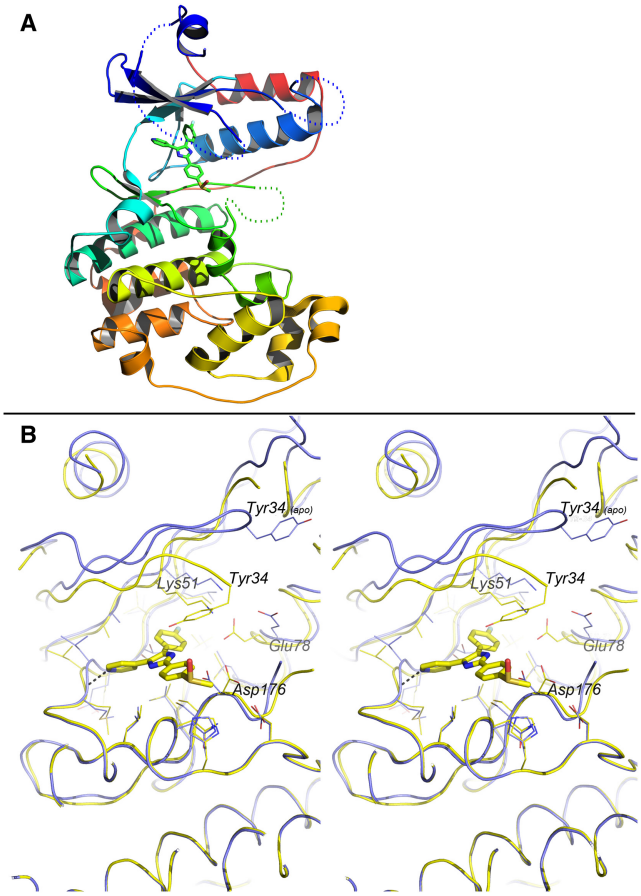

Figure 4. 3D Structure of LmaMPK10ΔC in Complex with SB203580

(A) Cartoon representation of LmaMPK10ΔC bound to the inhibitor SB203580. The model is colored according to a blue-to-red ramp, indicating the N-terminal to C-terminal sense of the polypeptide. The inhibitor is highlighted in stick representation colored according to atomic elements (oxygen, red; nitrogen, blue; carbon, green; sulfur, yellow; fluorine, sky blue). Dotted lines represent segments of the proteins that have not been included in the model because of poor or undetectable electron density.

(B) Superposition of LmaMPK10ΔC in its apo form (blue ribbon) and in complex with SB203580 (yellow), shown in stereo. The SB203580 is shown in stick representation colored by atom. The inhibitor-binding residues are shown in lines representation (colored by atom); for clarity only the ones displaying larger positional shifts are labeled. The single hydrogen bond between the nitrogen atoms of the pyrimidine ring on SB203580 and the main chain of Met115 is indicated in dotted lines. Note the closure movement in the inhibitor-bound structure, most prominently marked following the position of Tyr34, overall rotating the N-terminal lobe with respect to the C-terminal one, narrowing the nucleotide-binding cleft.

See also Figure S4.

the second half of the extension might physically reach the ATP-binding cleft, exerting the inhibition effect in nucleotide binding. ATP concentrations in the cell are typically high, and protein kinases have evolved a diverse array of molecular mechanisms to avoid potentially deleterious consequences of inappropriate activation. The particular ''locked-in'' architecture of LmaMPK10, with regard to the more canonical DFG-dependent Phe-flipping regulation away from the ATP-binding pocket, might be related to the appearance of a different regulation that maintains LmaMPK10 off until its self-peptide is outcompeted from the ATP-binding site.

EXPERIMENTAL PROCEDURES

Cloning and Mutagenesis

The sequences encoding for LmaMPK10 (full-length) and LmaMPKΔC (lacking the last 46 residues) were amplified by PCR and subcloned into plasmid pQE80 (Qiagen, Venlo, the Netherlands), previously modified to carry a Tobacco Etch Virus (TEV) protease cleavage site for removal of the N-terminal His-tag. Site-directed mutageneses were performed on the pQE80-LmaMPK10ΔC vector using specific 5′-phosphorylated primers and high-fidelity Phusion DNA polymerase (New England Biolabs Inc., Ipswich, MA, USA). Purified amplicons were incubated with DNA-ligase, and TOP10F' strain cells were transformed. Mutageneses were systematically confirmed by DNA sequence analysis. The N-terminal fusion of GFP to MPK10 in the leishmanial expression vector pXG has been described previously (Morales et al., 2007). The Lys51Ala mutation was introduced by PCR using the mutagenic primer 5′ ATTCCGGTCGCCATCgcGCGCGTGTTCAACAC 3′. Episomal tranfectants GFP-LmaMPK10 *wt* and GFP-LmaMPK10Lys51Ala were established by electroporation of 4 × 10^7 *L. donovani* LdB promastigotes from logarithmic culture with 20 μg of recombinant plasmid. Transfected cells were plated on media containing 20 μg/ml G418, and resistant colonies were expanded in liquid culture at drug concentrations up to 100 μg/ml G418.

Protein Expression

Transformed *E. coli* Top10F' cells were grown in Luria-Bertani medium supplemented with ampicillin (100 μg/ml) at 37°C until OD_{600} 0.8. Temperature was decreased to 20°C, and induction was triggered with 1 mM IPTG overnight. Cells were harvested by centrifugation at 2,000 g. Pellets were resuspended in 50 mM Tris.HCl (pH 8.5), 500 mM NaCl, supplemented with EDTA-free protease inhibitors (Roche, Indianapolis, IN, USA), and cells disrupted with lysozyme and sonication (five pulses of 30"). Soluble fractions were obtained by centrifugation for 30 min at 10,000 g.

Protein Purification

The soluble fraction of total protein extracts was immediately subjected to Ni^{2+} affinity chromatography (HisTrap, GE Healthcare Life Sciences, Waukesha, WI, USA), after adding 20 mM imidazole. Purified proteins were eluted with a linear gradient 4%–100% of Buffer B (50 mM Tris [pH 8.5], 500 mM NaCl, and 500 mM imidazole) in 15 column volumes. Fractions were pooled and incubated with TEV protease while dialyzed overnight against 50 mM Tris (pH 8.5) and 500 mM NaCl at 4°C. A second Ni^{2+} column purification step was performed. The flowthrough was collected and subjected to size-exclusion chromatography with a Superdex 26/60 75 prep (GE Healthcare Life Sciences) column previously equilibrated with 20 mM Tris (pH 8.5) and 150 mM NaCl. The peak fractions were pooled, concentrated to 10 mg/ml, and stored at 4°C until use.

Enzymatic Assays with Recombinant LmaMPK10ΔC

Radioactive kinase assays were performed in a total volume of 30 μl containing 500 ng purified recombinant LmaMPK10ΔC or LmaMPK10ΔC-Lys51Ala, kinase buffer (50 mM HEPES [pH 7.4], 10 mM MnCl2, 1 mM DTT, 20 mM β-glycerophosphate, and 0.1 mM NaVO4) and ATP (20 μM ATP and 5 μCi [γ^{32}P]-ATP). The reaction was incubated for 20 min at 30°C under constant agitation and stopped by the addition of 6 μl 6× Lämmli buffer. The reaction mixture was separated by SDS-PAGE. The gel was stained with Coomassie, dried, and subjected to autoradiography. Enzyme-coupled assays are detailed in the Supplemental Experimental Procedures.

Kinase Assay Using Leishmanial Recombinant Protein

L. donovani axenic amastigote cells were generated as detailed in the Supplemental Experimental Procedures. Total *L. donovani* protein extract (1–2 mg) was subjected to anti-GFP immunoprecipitation using the μMACS anti-GFP magnetic beads (Miltenyi Biotec, Bergisch-Gladbach, Germany #130-091-125). Immunoprecipitates were washed twice with 500 μl HNGT (20 mM HEPES [pH 7.4], 150 mM NaCl, 10% Glycerol, and 0.1% Triton

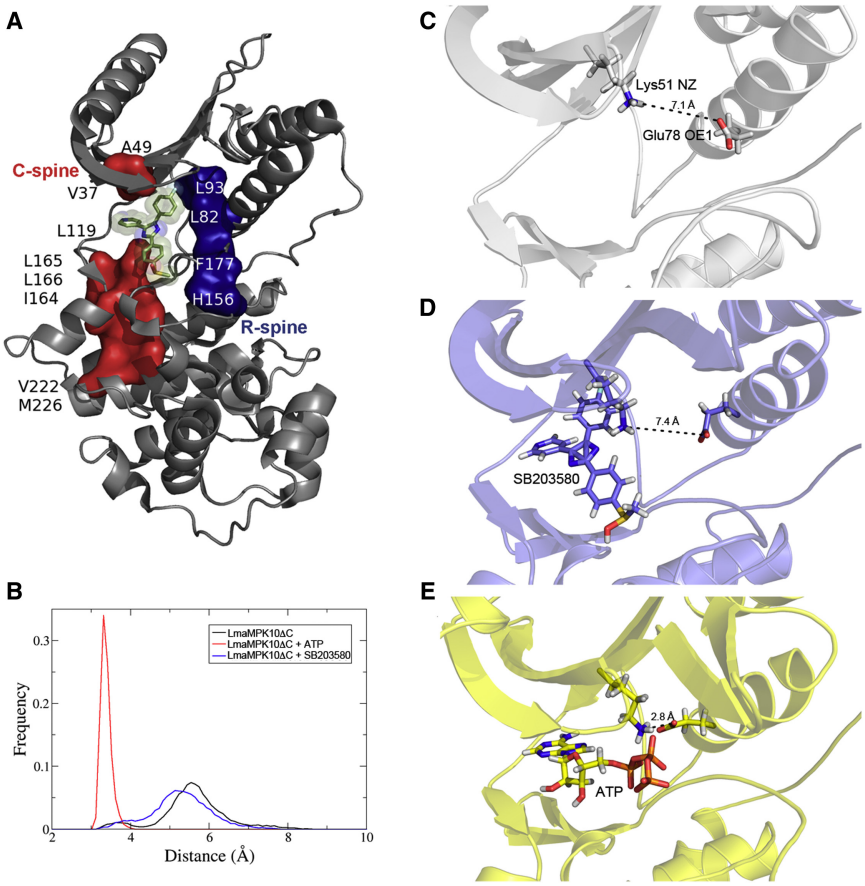

Figure 5. Activation State and Plasticity in LmaMPK10

(A) Catalytic and regulatory spines in LmaMPK10ΔC. Cartoon showing the LmaMPK10ΔC-SB203580 complex, with the inhibitor in stick and transparent molecular surface representation. Solid molecular surfaces are rendered for the labeled residues, composing the catalytic or C-spine (in red) and the regulatory or R-spine (in blue). Note the continuity in both spines, consistent with a "locked-in" active state architecture.

(B) Histogram of the interatomic distance from Lys51 NZ to Glu78 CD. Apo LmaMPK10ΔC, compared to structures bound to ATP and SB203580, are shown in different colors as labeled. The vertical axis is showing relative probability distance distributions. The distances along the simulations were collected and a probability distribution was generated every 0.1 Å, plotted relative to the total number of collected distances. As a control, independent molecular dynamics calculations were run from the same starting points as the complexed forms shown here but without adding the ligands, demonstrating that the starting structures do not affect the final outcome of the simulations (see Figure S5D).

(C) Cartoon representation of the final model of LmaMPK10ΔC after 100 ns molecular dynamics simulation, in its apo form, (D) in complex with SB203580, or (E) in complex with ATP. On these three panels, Lys51 and Glu78 are highlighted in sticks to show that only the occupation of ATP into the nucleotide-binding pocket predicts the triggering of the Lys51-Glu78 salt bridge (Lys51NZ-Glu78OE1 distances are indicated), with correlated P loop and αC helix conformational rearrangements.

See also Figure S5.

X-100) and twice with 500 μl kinase buffer (50 mM HEPES [pH 7.4], 10 mM MnCl2, 1 mM DTT, 20 mM β-glycerophosphate, and 0.1 mM $NaVO_4$). Twenty percent of the total volume was removed, boiled with Lämmli buffer, and subjected to SDS-PAGE and immunoblotting using anti-GFP antibodies. The remaining beads were drained and eluted from the columns in the absence of a magnetic field using 45 μl kinase buffer, and kinase reaction was started by the addition of 5 μl ATP/MBP mix (1 μCi/μl [γ-32P]-ATP, 200 μM rATP, and 1 μg/μl MBP). The reaction was incubated for 20 min at 30°C under constant agitation and stopped by the addition of 10 μl 6× Lämmli beads. The reaction mixture was separated by SDS-PAGE. The gel was stained with Coomassie, dried, and subjected to autoradiography. Immunoprecipitated GFP-LmaMPK10 *wt* and GFP-LmaMPK10Lys51Ala, barely detectable with Coomassie, were confirmed by western blotting onto polyvinylidene difluoride membranes (Millipore, Billerica, MA, USA). Proteins were revealed using mouse monoclonal anti-GFP horseradish peroxidase-conjugated antibody (Miltenyi Biotec, Teterow, Germany). After washing, blots were developed using SuperSignal chemiluminescent detection system (Pierce Protein Biology Products, Thermo Fisher Scientific Inc., Rockford, IL, USA) and visualized on X-ray film.

Crystallogenesis

Crystallization conditions were identified using JCSG Core Suit Screenings (Qiagen, Venlo, the Netherlands), with a robotic dispensing station (Honeybee963, Digilab) in 250 nl+250 nl sitting-drops (CrystalQuick 96-well, Greiner Bio-one, Frickenhausen, Germany) at 20°C. Conditions were optimized manually in hanging drops (VDX plates, Hampton Research, Aliso Viejo, CA, USA), mixing 2 μl of protein solution (10 mg/ml) and 2 μl of reservoir solution containing: 0.1 M HEPES (pH 7.5), 12% PEG 4000, 5% glycerol, and 5% isopropanol. Crystals of apo-LmaMPK10ΔC appeared after 4 days. The LmaMPK10ΔC-SB203580 complex was prepared by overnight soaking of LmaMPK10ΔC crystals in mother liquor containing 4 mM SB203580 (Sigma-Aldrich, St. Louis, MO, USA).

X-Ray Diffraction Data Collection, Processing, Structure Determination, and Refinement

Single crystals were cryoprotected in mother liquor containing 20% glycerol and frozen in liquid N_2. X-ray diffraction data were collected at 100°K (Cryostream Series700, Oxford Cryosystems, Oxford, UK) using a rotating anode X-ray generator (Micromax007-HF, Rigaku, The Woodlands, TX, USA) equipped with Varimax-HF (Rigaku) multilayer optics and a Mar345 (Mar Research, Norderstedt, Germany) image plate detector. Data sets were processed using Mosflm/Scala (Collaborative Computational Project Number 4, 1994). Molecular replacement was used to obtain initial phases, using the program AMoRe (Trapani and Navaza, 2008). The structure of human p38α (PDB ID code 3HV3) was used as search probe. Cycles of reciprocal space refinement were performed with the program Buster (Bricogne et al., 2011), alternated with manual rebuilding and validation (Emsley and Cowtan, 2004). Visualization, analysis, and figure preparation was done with Pymol (DeLano, 2002), and electrostatic potential maps were calculated with the program APBS (Baker et al., 2001).

Isothermal Titration Calorimetry

The association of LmaMPK10 and LmaMPK10ΔC to SB203580 was quantified by isothermal titration calorimetry using a high-precision VP-ITC isothermal titration calorimetric (MicroCal Inc., Piscataway, NJ, USA). Purified LmaMPK10 (34 μM) or LmaMPK10ΔC (3 μM) were diluted in 20 mM Tris (pH 8.5), 50 mM NaCl, and 0.8% DMSO. SB203580 was diluted in the same buffer and used at 450 μM for LmaMPK10 or at 45 μM for LmaMPK10ΔC. Solutions were thoroughly degassed under gentle vacuum at 30°C. Experimental

setup consisted of repeated injections of SB203580 into the calorimetric cell containing LmaMPK10 or LmaMPK10ΔC. Experiments were performed at 30°C with a preinjection of 1μl followed by 29 injections of 10 μl spaced by 360 s and using a 394 rpm rotating syringe. See Supplemental Experimental Procedures for further details on data processing.

SUPPLEMENTAL INFORMATION

Supplemental Information includes five figures and Supplemental Experimental Procedures and can be found with this article online at http://dx.doi.org/10.1016/j.str.2012.07.005.

ACKNOWLEDGMENTS

This work was supported by the Seventh Framework Programme of the European Commission through a grant to the LEISHDRUG Project (223414) and ECOS-Sud/ECOS-Uruguay (PU11B02). We thank Analía Lima and Carlos Batthyány (Analytical Biochemistry and Proteomics Unit) and Horacio Botti (Unit of Protein Crystallography), Institut Pasteur de Montevideo, for helpful discussions and MS analyses and Rosario Duran (Analytical Biochemistry and Proteomics Unit) for her generous gift of PknB and GarA for kinase activity controls. We also acknowledge Ahmed Haouz (Crystallogenesis and X-ray Diffraction facility) and Jacques d'Alayer (Protein Microsequencing and Analysis facility), Institut Pasteur, for their helpful assistance.

Received: March 15, 2012
Revised: June 23, 2012
Accepted: July 9, 2012
Published online: August 9, 2012

REFERENCES

Adams, P.D., Afonine, P.V., Bunkóczi, G., Chen, V.B., Davis, I.W., Echols, N., Headd, J.J., Hung, L.W., Kapral, G.J., Grosse-Kunstleve, R.W., et al. (2010). PHENIX: a comprehensive Python-based system for macromolecular structure solution. Acta Crystallogr. D Biol. Crystallogr. *66*, 213–221.

Baker, N.A., Sept, D., Joseph, S., Holst, M.J., and McCammon, J.A. (2001). Electrostatics of nanosystems: application to microtubules and the ribosome. Proc. Natl. Acad. Sci. USA *98*, 10037–10041.

Bellon, S., Fitzgibbon, M.J., Fox, T., Hsiao, H.M., and Wilson, K.P. (1999). The structure of phosphorylated p38gamma is monomeric and reveals a conserved activation-loop conformation. Structure *7*, 1057–1065.

Bengs, F., Scholz, A., Kuhn, D., and Wiese, M. (2005). LmxMPK9, a mitogen-activated protein kinase homologue affects flagellar length in Leishmania mexicana. Mol. Microbiol. *55*, 1606–1615.

Bhattacharya, P., Gupta, G., Majumder, S., Adhikari, A., Banerjee, S., Halder, K., Majumdar, S.B., Ghosh, M., Chaudhuri, S., Roy, S., and Majumdar, S. (2011). Arabinosylated lipoarabinomannan skews Th2 phenotype towards Th1 during Leishmania infection by chromatin modification: involvement of MAPK signaling. PLoS ONE *6*, e24141.

Bricogne, G., Blanc, E., Brandl, M., Flensburg, C., Keller, P., Paciorek, W., Roversi, P., Sharff, A., Smart, O.S., Vonrhein, C., et al. (2011). BUSTER version 2.8.0 (Cambridge, United Kingdom: Global Phasing Ltd.).

Brumlik, M.J., Pandeswara, S., Ludwig, S.M., Murthy, K., and Curiel, T.J. (2011). Parasite mitogen-activated protein kinases as drug discovery targets to treat human protozoan pathogens. J. Signal Transduct. *2011*, 971968.

Chen, G., Porter, M.D., Bristol, J.R., Fitzgibbon, M.J., and Pazhanisamy, S. (2000). Kinetic mechanism of the p38-alpha MAP kinase: phosphoryl transfer to synthetic peptides. Biochemistry *39*, 2079–2087.

Chen, V.B., Arendall, W.B., 3rd, Headd, J.J., Keedy, D.A., Immormino, R.M., Kapral, G.J., Murray, L.W., Richardson, J.S., and Richardson, D.C. (2010). MolProbity: all-atom structure validation for macromolecular crystallography. Acta Crystallogr. D Biol. Crystallogr. *66*, 12–21.

Chuderland, D., Konson, A., and Seger, R. (2008). Identification and characterization of a general nuclear translocation signal in signaling proteins. Mol. Cell *31*, 850–861.

Collaborative Computational Project, Number 4. (1994). The CCP4 suite: programs for protein crystallography. Acta Crystallogr. D Biol. Crystallogr. *50*, 760–763.

Cuenda, A., Rouse, J., Doza, Y.N., Meier, R., Cohen, P., Gallagher, T.F., Young, P.R., and Lee, J.C. (1995). SB 203580 is a specific inhibitor of a MAP kinase homologue which is stimulated by cellular stresses and interleukin-1. FEBS Lett. *364*, 229–233.

DeLano, W.L. (2002) The PyMOL Molecular Graphics System DeLano Scientific, San Carlos, CA, USA. http://www.pymol.org.

Emsley, P., and Cowtan, K. (2004). Coot: model-building tools for molecular graphics. Acta Crystallogr. D Biol. Crystallogr. *60*, 2126–2132.

Huse, M., and Kuriyan, J. (2002). The conformational plasticity of protein kinases. Cell *109*, 275–282.

Johnson, L.N. (2009). Protein kinase inhibitors: contributions from structure to clinical compounds. Q. Rev. Biophys. *42*, 1–40.

Kannan, N., and Neuwald, A.F. (2004). Evolutionary constraints associated with functional specificity of the CMGC protein kinases MAPK, CDK, GSK, SRPK, DYRK, and CK2alpha. Protein Sci. *13*, 2059–2077.

Kannan, N., Taylor, S.S., Zhai, Y., Venter, J.C., and Manning, G. (2007). Structural and functional diversity of the microbial kinome. PLoS Biol. *5*, e17.

Kornev, A.P., Haste, N.M., Taylor, S.S., and Eyck, L.F. (2006). Surface comparison of active and inactive protein kinases identifies a conserved activation mechanism. Proc. Natl. Acad. Sci. USA *103*, 17783–17788.

Kramer, S. (2012). Developmental regulation of gene expression in the absence of transcriptional control: the case of kinetoplastids. Mol. Biochem. Parasitol. *181*, 61–72.

Kumari, S., Singh, S., Saha, B., and Paliwal, P.K. (2011). Leishmania major MAP kinase 10 is protective against experimental L. major infection. Vaccine *29*, 8783–8787.

Manning, G., Whyte, D.B., Martinez, R., Hunter, T., and Sudarsanam, S. (2002). The protein kinase complement of the human genome. Science *298*, 1912–1934.

Morales, M.A., Renaud, O., Faigle, W., Shorte, S.L., and Späth, G.F. (2007). Over-expression of Leishmania major MAP kinases reveals stage-specific induction of phosphotransferase activity. Int. J. Parasitol. *37*, 1187–1199.

Morales, M.A., Watanabe, R., Laurent, C., Lenormand, P., Rousselle, J.C., Namane, A., and Späth, G.F. (2008). Phosphoproteomic analysis of Leishmania donovani pro- and amastigote stages. Proteomics *8*, 350–363.

Naula, C., Parsons, M., and Mottram, J.C. (2005). Protein kinases as drug targets in trypanosomes and Leishmania. Biochim. Biophys. Acta *1754*, 151–159.

Neuber, H. (2008). Leishmaniasis. J. Dtsch. Dermatol. Ges. *6*, 754–765.

Ojo, K.K., Arakaki, T.L., Napuli, A.J., Inampudi, K.K., Keyloun, K.R., Zhang, L., Hol, W.G., Verlinde, C.L., Merritt, E.A., and Van Voorhis, W.C. (2011). Structure determination of glycogen synthase kinase-3 from Leishmania major and comparative inhibitor structure-activity relationships with Trypanosoma brucei GSK-3. Mol. Biochem. Parasitol. *176*, 98–108.

Pargellis, C., Tong, L., Churchill, L., Cirillo, P.F., Gilmore, T., Graham, A.G., Grob, P.M., Hickey, E.R., Moss, N., Pav, S., and Regan, J. (2002). Inhibition of p38 MAP kinase by utilizing a novel allosteric binding site. Nat. Struct. Biol. *9*, 268–272.

Parsons, M., Worthey, E.A., Ward, P.N., and Mottram, J.C. (2005). Comparative analysis of the kinomes of three pathogenic trypanosomatids: Leishmania major, Trypanosoma brucei and Trypanosoma cruzi. BMC Genomics *6*, 127.

Plotnikov, A., Chuderland, D., Karamansha, Y., Livnah, O., and Seger, R. (2011a). Nuclear extracellular signal-regulated kinase 1 and 2 translocation is mediated by casein kinase 2 and accelerated by autophosphorylation. Mol. Cell. Biol. *31*, 3515–3530.

Plotnikov, A., Zehorai, E., Procaccia, S., and Seger, R. (2011b). The MAPK cascades: signaling components, nuclear roles and mechanisms of nuclear translocation. Biochim. Biophys. Acta *1813*, 1619–1633.

Rotureau, B., Morales, M.A., Bastin, P., and Späth, G.F. (2009). The flagellum-mitogen-activated protein kinase connection in Trypanosomatids: a key sensory role in parasite signalling and development? Cell. Microbiol. *11*, 710–718.

Scheeff, E.D., and Bourne, P.E. (2005). Structural evolution of the protein kinase-like superfamily. PLoS Comput. Biol. *1*, e49.

Schindler, T., Bornmann, W., Pellicena, P., Miller, W.T., Clarkson, B., and Kuriyan, J. (2000). Structural mechanism for STI-571 inhibition of abelson tyrosine kinase. Science *289*, 1938–1942.

Simard, J.R., Getlik, M., Grütter, C., Pawar, V., Wulfert, S., Rabiller, M., and Rauh, D. (2009). Development of a fluorescent-tagged kinase assay system for the detection and characterization of allosteric kinase inhibitors. J. Am. Chem. Soc. *131*, 13286–13296.

Taylor, S.S., and Radzio-Andzelm, E. (1994). Three protein kinase structures define a common motif. Structure *2*, 345–355.

Taylor, S.S., and Kornev, A.P. (2011). Protein kinases: evolution of dynamic regulatory proteins. Trends Biochem. Sci. *36*, 65–77.

Technikova-Dobrova, Z., Sardanelli, A.M., and Papa, S. (1991). Spectrophotometric determination of functional characteristics of protein kinases with coupled enzymatic assay. FEBS Lett. *292*, 69–72.

Thévenet, P., Shen, Y., Maupetit, J., Guyon, F., Derreumaux, P., and Tufféry, P. (2012). PEP-FOLD: an updated de novo structure prediction server for both linear and disulfide bonded cyclic peptides. Nucleic Acids Res. *40* (Web Server issue), W288–W293.

Trapani, S., and Navaza, J. (2008). AMoRe: classical and modern. Acta Crystallogr. D Biol. Crystallogr. *64*, 11–16.

Turjanski, A.G., Hummer, G., and Gutkind, J.S. (2009). How mitogen-activated protein kinases recognize and phosphorylate their targets: A QM/MM study. J. Am. Chem. Soc. *131*, 6141–6148.

Wiese, M. (1998). A mitogen-activated protein (MAP) kinase homologue of Leishmania mexicana is essential for parasite survival in the infected host. EMBO J. *17*, 2619–2628.

Wiese, M. (2007). Leishmania MAP kinases—familiar proteins in an unusual context. Int. J. Parasitol. *37*, 1053–1062.

Xie, X., Gu, Y., Fox, T., Coll, J.T., Fleming, M.A., Markland, W., Caron, P.R., Wilson, K.P., and Su, M.S. (1998). Crystal structure of JNK3: a kinase implicated in neuronal apoptosis. Structure *6*, 983–991.

Yang, Z., Zhang, X., Darrah, P.A., and Mosser, D.M. (2010). The regulation of Th1 responses by the p38 MAPK. J. Immunol. *185*, 6205–6213.

Zhang, Y.Y., Mei, Z.Q., Wu, J.W., and Wang, Z.X. (2008). Enzymatic activity and substrate specificity of mitogen-activated protein kinase p38alpha in different phosphorylation states. J. Biol. Chem. *283*, 26591–26601.

